International Journal of
Environmental Research and Public Health

MDPI

Article

Removal of Ammonia Using Persulfate during the Nitrate Electro-Reduction Process

Shuai Yang [1], Xinxin Hu [2], Xinyu You [1], Wenwen Zhang [1], Yu Liu [1] and Wenyan Liang [1,*]

[1] Beijing Key Laboratory for Source Control Technology of Water Pollution, College of Environmental Science and Engineering, Beijing Forestry University, Beijing 100083, China; ysbjfu@163.com (S.Y.); yxybjfu@163.com (X.Y.); zhang_wen0902@163.com (W.Z.); liuyubjfu@163.com (Y.L.)
[2] Water Quality Testing Center, Beijing Drainage Water Environment Development Co., Ltd., Beijing 100022, China; xinxinhu@126.com
* Correspondence: lwy@bjfu.edu.cn; Fax: +86-10-6233-6615

Abstract: NH_4^+ is often produced during the electro-reduction of NO_3^-, which results in inadequate total nitrogen (TN) removal during advanced sewage treatment. In this study, the electro-reduction byproduct NH_4^+ was oxidized and removed using sulfate radical ($SO_4^{\bullet-}$)-based advanced oxidation. Persulfate (PS) was activated by electrocatalysis, using Co/$AC_{0.9}$-$AB_{0.1}$ particle electrodes to produce $SO_4^{\bullet-}$. Results showed that when the influent concentration of NO_3^--N was 20 mg/L, a PS dosage of 5.0 mM could completely oxidize NH_4^+ at 0.1 A (nondetectable in effluent) reducing the TN concentration from 9.22 to 0.55 mg/L. The presence of coexisting PO_4^{3-}, CO_3^{2-} and humic acid suppressed the oxidation and removal of NH_4^+. Electron spin resonance (ESR) spectra and quenching experiments revealed $SO_4^{\bullet-}$ as the dominant radical in the process of indirect NH_4^+ oxidation, while •OH radicals only had an assisting role, and the surface accumulated free radicals were responsible for the indirect oxidation of NH_4^+. Cyclic voltammetry (CV) curves indicated that NO_3^- was primarily reduced via atomic H*-mediated indirect reduction. Therefore, the activation of PS using Co/$AC_{0.9}$-$AB_{0.1}$ particle electrodes might be a promising alternative method for oxidizing byproduct NH_4^+ in the electro-reduction of NO_3^- and reduce TN concentration in advanced sewage treatment.

Keywords: ammonia; persulfate; electro-oxidation; particle electrode

check for updates

Citation: Yang, S.; Hu, X.; You, X.; Zhang, W.; Liu, Y.; Liang, W. Removal of Ammonia Using Persulfate during the Nitrate Electro-Reduction Process. *Int. J. Environ. Res. Public Health* **2022**, *19*, 3270. https://doi.org/10.3390/ijerph19063270

Academic Editor: Paul B. Tchounwou

Received: 13 February 2022
Accepted: 8 March 2022
Published: 10 March 2022

Publisher's Note: MDPI stays neutral with regard to jurisdictional claims in published maps and institutional affiliations.

Copyright: © 2022 by the authors. Licensee MDPI, Basel, Switzerland. This article is an open access article distributed under the terms and conditions of the Creative Commons Attribution (CC BY) license (https://creativecommons.org/licenses/by/4.0/).

1. Introduction

The total nitrogen (TN) content of the effluent of most sewage treatment plants can reach as high as 10 mg/L, even after primary and secondary treatment [1]. In sewage wastewater, TN is mainly composed of NO_3^-, with a small amount of NH_3/NH_4^+ [2]. It has been well established that NO_3^- and NH_4^+ bear a negative impact on aquatic environments, such as eutrophication and the occurrence of algal blooms [3]. Therefore, advanced treatment methods are required to reduce the TN content of sewage.

Electrochemical reduction is a feasible option for the conversion of NO_3^- to N_2, with the benefits of simple operational methods, low-environmental impact and economic efficiency [4]. The electro-reduction of NO_3^- occurs via a complex process involving multi-electron transfer between the different valence states of nitrogen and its reaction products, such as N_2H_4, NH_3, NH_2OH, N_2, N_2O, NO, NO_2^-, and NO_2 [5]. Direct reduction and indirect reduction pathways have both been shown to be involved in the electro-reduction of NO_3^- [6]. During the direct reduction process, NO_3^- is first adsorbed onto the electrode and then converted to $NO_3^-{}_{(ad)}$. Electron transfer leads to the generation of $NO_3^{2-}{}_{(ad)}$, $NO_2^-{}_{(ad)}$ and other short-lived intermediates [7]. Subsequently, $NO_3^{2-}{}_{(ad)}$ and $NO_2^-{}_{(ad)}$ are converted (in a stepwise reduction process) to $NO_{(ad)}$, then finally to N_2 and NH_4^+, sometimes via the intermediates N_2O, NH_2OH and N_2H_4 [5]. The indirect reduction process refers to atomic H*-mediated reactions, where cathode surface-adsorbed atomic H* is produced via the reduction of protons. The products formed during the indirect reduction process usually include NO_2^-, NO, N_2,

and NH_3/NH_4^+ [8]. Although NO_2^- exists as the product of the rate-limiting step in both direct and indirect reduction, it can be rapidly degraded and converted to N_2 and NH_4^+ [9]. Therefore, the nitrogen substances present in solution after electro-reduction mainly consist of the NH_3/NH_4^+ product and residual NO_3^-. However, the production of NH_4^+ presents a problem as it is a very stable nitrogen intermediate, not only reducing the denitrification efficiency of the treatment system, but also posing a threat to the aquatic environment due to its hepatotoxicity and nephrotoxicity [10].

At present, the systems used for NO_3^- electro-reduction include traditional two-dimensional (2D) anode/cathode plate systems and the newly-developed three-dimensional (3D) particle electrode bed system [7]. In both systems, the electrode material significantly influences the efficiency of NO_3^- electro-reduction [11]. The electrode materials used in 2D systems usually include monometallic (Cu, Ni, Al, Pd, Pt, Pb, Ti, and Rh [12–14]) and bimetallic (Cu-Ni, Cu-Sn, Sn-Pd, Cu-Pd, and Cu-Zn [15–18]) catalytic electrodes. For 3D systems, the particle electrodes are composed of a carrier material loaded with a catalyst, such as Co_3O_4-TiO_2/Ti, PdCu@OMC (OMC: ordered mesoporous carbon), Pd-Sn/AC, Cu/AC or Co/$AC_{0.9}$-$AB_{0.1}$ (AC: active carbon, AB: acetylene black) [9,19–22]. Compared to the 2D system, the addition of particle electrodes results in an increased specific surface area and availability of reactive sites, while also shortening the mass transfer distance, which enhances the removal efficiency and reaction rate [7,23]. However, accumulation of byproduct NH_4^+ also occurs in the 3D system [22]. In order to remove NH_4^+, chlorine active species are often applied, such as ClO^-, $HClO^{\bullet-}$ and $Cl_2^{\bullet-}$, which are generated via electrochemical reactions [24]. However, the removal efficiency highly depends on the concentration of Cl^-, with either excessive or insufficient dosages reducing the removal effect. Moreover, Cl^- easily combines with organic matter and generates chlorination byproducts, such as trihalomethanes, trichloromethane and haloacetic acids, which present a secondary threat to the health of aquatic ecosystems and human populations [25]. The role of hydroxyl radicals (•OH) in the oxidization of NH_4^+ has also been investigated [5]. However, the rate of reaction between •OH and ammonia is slow, reducing the overall removal efficiency [26].

Persulfate (PS) oxidation technology has recently attracted increasing attention [27]. Sulfate radicals ($SO_4^{\bullet-}$) are generated from the activation of PS under the influence of UV radiation, increased temperatures, magnetic fields and electrical currents [28,29]. In comparison, $SO_4^{\bullet-}$ possesses a higher redox potential (2.5–3.1 V) than •OH (1.8–2.7 V), as well as a longer half-life (30–40 μs for $SO_4^{\bullet-}$ and 20 ns for •OH), wider pH range (2–8 for $SO_4^{\bullet-}$ and 2–4 for •OH) and a lower O−O bond breaking energy (140 kJ/mol for $SO_4^{\bullet-}$ and 213.3 kJ/mol for •OH) [27,30]. As an electrophilic species, $SO_4^{\bullet-}$ tends to react with alkoxy (-OR), amino (-NH_2), and hydroxyl (-OH) groups [31]. $SO_4^{\bullet-}$-based advance oxidation has been used previously in the field of landfill leachate treatment, to remove NH_4^+ and gaseous ammonia [32]. Therefore, in the present study, NH_4^+ removal was assessed using persulfate in a 3D PS-Co/$AC_{0.9}$-$AB_{0.1}$ system, with the aim of increasing TN removal. The effects of various operational parameters were assessed, allowing the nitrogen conversion pathway and the denitrification mechanism to be investigated. Furthermore, electrocatalytic denitrification was also carried out using Cl^- in a comparative system.

2. Materials and Methods

2.1. Experimental Setup

As shown in Figure 1, the mesh plates composed of Ti/RuO_2 (12 × 2.5 cm^2) and Ti (12 × 2.5 cm^2) in rectangular cells were obtained from Hengli Ti Co., Ltd. (Beijing, China), for use as the anode and cathode, respectively. Then, 15 g of particle electrodes were packed between the two mesh plates (total L × W × H = 2.5 × 2.4 × 12 cm^3). Simulated wastewater with PS dosing (namely $K_2S_2O_8$) was continuously pumped into the reactor and treated without circulation.

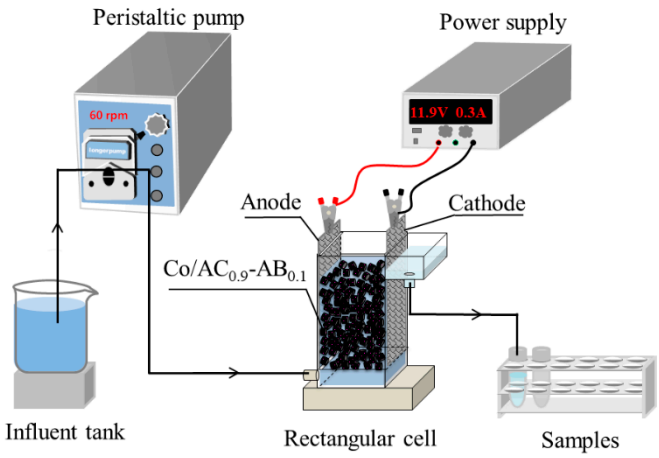

Figure 1. The schematic diagram for ammonia removal using electric activation of persulfate during the nitrate electro-reduction process. $Co/AC_{0.9}$-$AB_{0.1}$ particle electrodes are packed between a pair of anode and cathode mesh plates.

2.2. Preparation of Particle Electrodes

The preparation of particle electrodes was performed according to a previously reported method [22]. Briefly, 90 g of powdered activated carbon (AC) and 10 g of powdered acetylene black (AB) were impregnated into 300 mL $Co(NO_3)_2$ (0.4 mol/L) and 100 mL distilled water, respectively. Then, AC and AB were separated by centrifugation and dried at 105 °C. The dried AC and AB samples were mixed thoroughly using polyvinyl alcohol as an adhesive at a mass ratio of 9:1, then molded into small cylindrical granules (~$\Phi \times H = 4$ mm $\times$ 5 mm) using a granulator. After drying at 105 °C for 24 h, the $Co/AC_{0.9}$-$AB_{0.1}$ particles were calcinated in a muffle furnace at 600 °C for 4 h under an N_2 atmosphere.

2.3. Experimental Procedure

The simulated wastewater was prepared by dissolving KNO_3 in distilled water (NO_3^--N = 20 mg/L), using 10.0 mM Na_2SO_4 as an electrolyte. After 120 min, adsorption reached saturation point and the electrical current was turned on. During the study of PS dosage, PS doses were applied from 1.5–5.0 mM. The treatments were carried out under successive currents of 0.1, 0.2, 0.3, and 0.4 A for 2 h/each current. Particle electrodes were replaced with new ones after each group treatment from 0.1–0.4 A. To investigate the effects of coexisting substances, the current was set at 0.3 A and the PS dosage remained constant at 5.0 mM. The concentrations of PO_4^{3-}-P and CO_3^{2-}-C ranged from 0.5–3.0 mg/L and 50.0–200.0 mg/L, respectively. The humic acid (HA) was used to simulate the dissolved organic matter. The concentration of HA was expressed by chemical oxygen demand, namely 50.0–120.0 mg COD/L (COD) in the experiments. Therefore, the concentration of HA was expressed by COD, respectively. Particle electrodes were replaced with new ones after treatment for each coexisting substance. The hydraulic retention time (HRT) remained constant at 60 min for all experiments. To assess the comparative effect of Cl^-, the dosage of Cl^- was varied from 1.5–5.0 mM, while all other conditions remained the same as described for PS experiments. Samples were collected from the outlet at 20 min intervals for the detection of NO_3^--N, NO_2^--N, NH_4^+-N, and $S_2O_8^{2-}$. The experiments under initial 20 mg/L NO_3^--N and without PS dosing were used as controls.

2.4. Identification of Reactive Species and Dominant Radicals

Free radicals were determined and recorded using an electron spin resonance (ESR) spectrometer (EMX Plus, Bruker, Karlsruhe, Germany). The parameter settings included a center field of 3513 G, seep width of 100 G, microwave power of 20 mW, and a scan time of 60 s [33]. The test samples were mixed with 50 mM 5,5-dimethyl-1-pyrrolidine N-oxide (DMPO, TCI Development, Tokyo, Japan). Quenching experiments were performed to identify the contribution of different radical species using simulated wastewater, composed

of 5.0 mM PS in 6.0 mg/L NH_4^+-N in distilled water, using different molar ratios of [scavenger]/[PS] to screen free radicals and establish their contributions. Molar ratios of 1000:1 tert-butyl alcohol (TBA, ≥99%), 1000:1 and 2000:1 ethanol (EtOH, ≥99%) and 200:1 phenol (≥99%) were separately added to simulated sewage samples prior to treatment. Due to the potential interference caused by organic reagents, samples were filtered through a 0.22 μm membrane prior to NH_4^+ determination.

2.5. Analytical Methods

NO_3^- and NO_2^- were determined via ion chromatography (Dionex ICS-3000, Sunnyvale, CA, USA) using a Dionex IonPac AS11-HC analytical column (4 mm × 250 mm) and an AG11-HC guard column (4 mm × 40 mm). Elution was performed using 12.5 mM NaOH at a flow rate of 1.0 mL/min. NH_4^+ was analyzed using salicylic acid spectrophotometry (UV2600, Techocomp, Beijing, China) [34]. Total nitrogen (TN) was calculated as the sum of NO_3^--N, NO_2^--N and NH_4^+-N. The pH value was determined using a pH-meter (PB-10, BSISL, China). $S_2O_8^{2-}$ was determined by UV spectrophotometry [35]. The activation efficiency of PS was calculated according to Equation (1), as follows:

$$\text{PS activation efficiency} \approx \frac{C_0 - C_t}{C_0} \times 100\% \quad (1)$$

where, C_0 and C_t are the PS concentration of the influent and effluent, respectively.

2.6. Electrochemical Measurements

Cyclic voltammetry (CV) measurements were performed using an electrochemical workstation (CHI 660D, Shanghai CH Instruments, China), with Pt filament and Ag/AgCl electrodes employed as the counter and reference electrodes, respectively. A glassy carbon disk electrode (3.0 mm) was used as the working electrode. Approximately 20.0 μL of pre-dispersed catalyst ink was coated dropwise onto the polished glassy carbon electrode. CV tests were performed with a cycle ranging from −0.39 V to +1.61 V and a scan rate of 0.1 V/s for 10 segments. A solution containing 0.5 M Na_2SO_4 was used as the supporting electrolyte. All solutions were prepared using ultrapure water and purged with N_2 gas for 20 min prior to measurements. The potentials were established in reference to a reversible hydrogen electrode (RHE).

2.7. Statistical Analysis

The one-way analysis of variance (ANOVA) was carried out using IBM SPSS v.20.0 (SPSS Inc., Chicago, IL, USA) software. Unless otherwise stated, results were considered to indicate significant differences if $p < 0.05$.

3. Results and Discussion

3.1. Nitrogen Conversion and Removal under Different PS Dosage and Current Conditions

As shown in Figure 2, the Co/$AC_{0.9}$-$AB_{0.1}$ particle electrodes exhibited excellent catalytic activity for the electro-reduction of NO_3^-. For samples without PS dosing, the percentage of NO_3^- conversion reached 80.5–90.2%, with the percentage conversion increasing in accordance with the applied current. This phenomenon occurred due to Co on the surface of particle electrodes having a strong catalytic activity for the production of atomic H*, which was beneficial to the indirect reduction of NO_3^- [22]. Following the addition of PS at dosages of 1.5–5.0 mM, NO_3^- reduction was further increased by 9.4–16.7%. Although PS activation occurred at the cathodic side of the particle electrode [36], the PS activation process did not interfere with the reduction of NO_3^-. PS is frequently used in advanced oxidation processes, but it can also facilitate the formation of Co-H* on electrode surfaces [36]. Therefore, PS promotes the atomic H*-mediated reduction of NO_3^-. Compared with the control samples, the addition of 1.5 mM PS significantly enhanced the reduction of NO_3^- at 0.2–0.4 A ($p < 0.05$), although this effect was not observed at 0.1 A. When the PS dosage was increased further to 3.0 and 5.0 mM, the enhancement effect was

significantly greater than that of 1.5 mM PS ($p < 0.05$). However, there were no significant differences found between 3.0 and 5.0 mM ($p > 0.05$), implying that increases in the dosage of PS beyond 3.0 mM, did not further improve NO_3^- reduction.

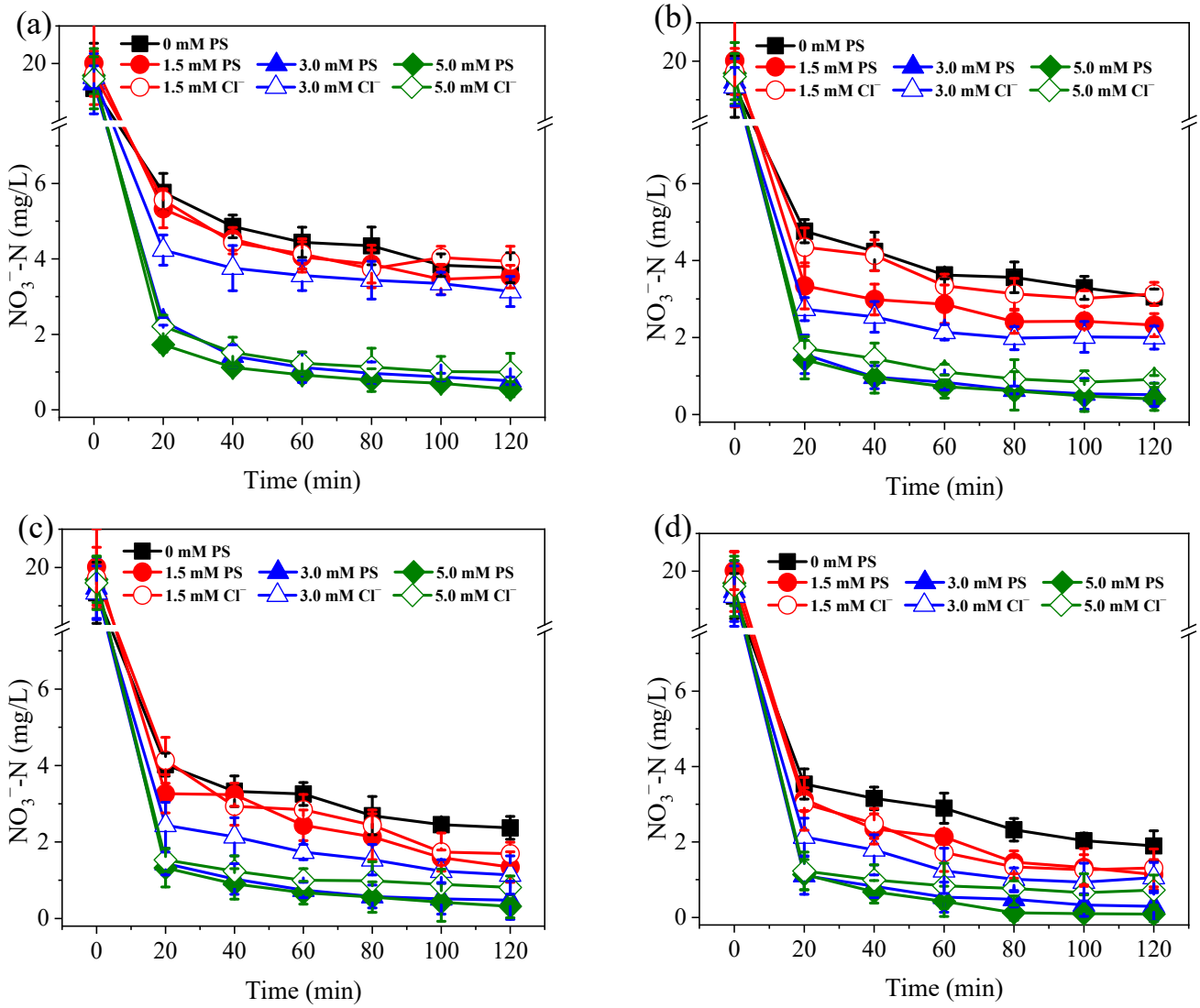

Figure 2. Variation of NO_3^--N concentration under currents of 0.1 A (**a**), 0.2 A (**b**), 0.3 A (**c**), and 0.4 A (**d**). The dosage of PS and Cl^- were all set at 1.5–5.0 mM. Initial NO_3^--N was 20 mg/L. The 10.0 mM Na_2SO_4 was used as electrolyte.

During the electro-reduction process at 0.1–0.4 A, approximately 10.2–28.2% of NO_3^- was converted into NH_4^+ without PS dosing (Figure 3). Therefore, when the influent NO_3^--N concentration was ~20.0 mg/L, 2.1–5.5 mg/L of NH_4^+-N was discharged into the effluent. It is known that NH_4^+-N concentrations over 2.0 mg/L can cause toxicity to aquatic life, such as fish [37]. However, compared with controls, the NH_4^+-N concentration was significantly reduced after PS dosing at all assessed currents ($p < 0.05$). Even low current conditions of 0.1 A, and the addition of 5.0 mM PS resulted in NH_4^+ being undetectable in the effluent. In contrast, when 5.0 mM of Cl^- was added to the system, the concentration of NH_4^+ in the effluent continually accumulated throughout the whole experimental process, reaching 4.7 mg/L. As can be seen from Figure 4, the PS activation efficiency reached >94.1% at 0.1 A, suggesting that PS can easily be activated by Co/$AC_{0.9}$-$AB_{0.1}$ particle electrodes. Due to the effective activation of PS, the oxidation of NH_4^+ was positively correlated with PS dosage, with higher PS dosages achieving a better NH_4^+ oxidation

efficiency. Furthermore, increases in current could overcome the effects of low PS dosage, with a current of 0.3 A resulting in NH_4^+ being undetectable in the effluent at a PS dose of 3.0 mM. When 3.0 mM Cl^- was applied, the effluent still contained 2.8 mg/L NH_4^+-N. Although active chlorine species have the capacity to oxidize NH_4^+, they cannot oxidize and remove NH_4^+ as efficiently as PS at an equivalent dosage.

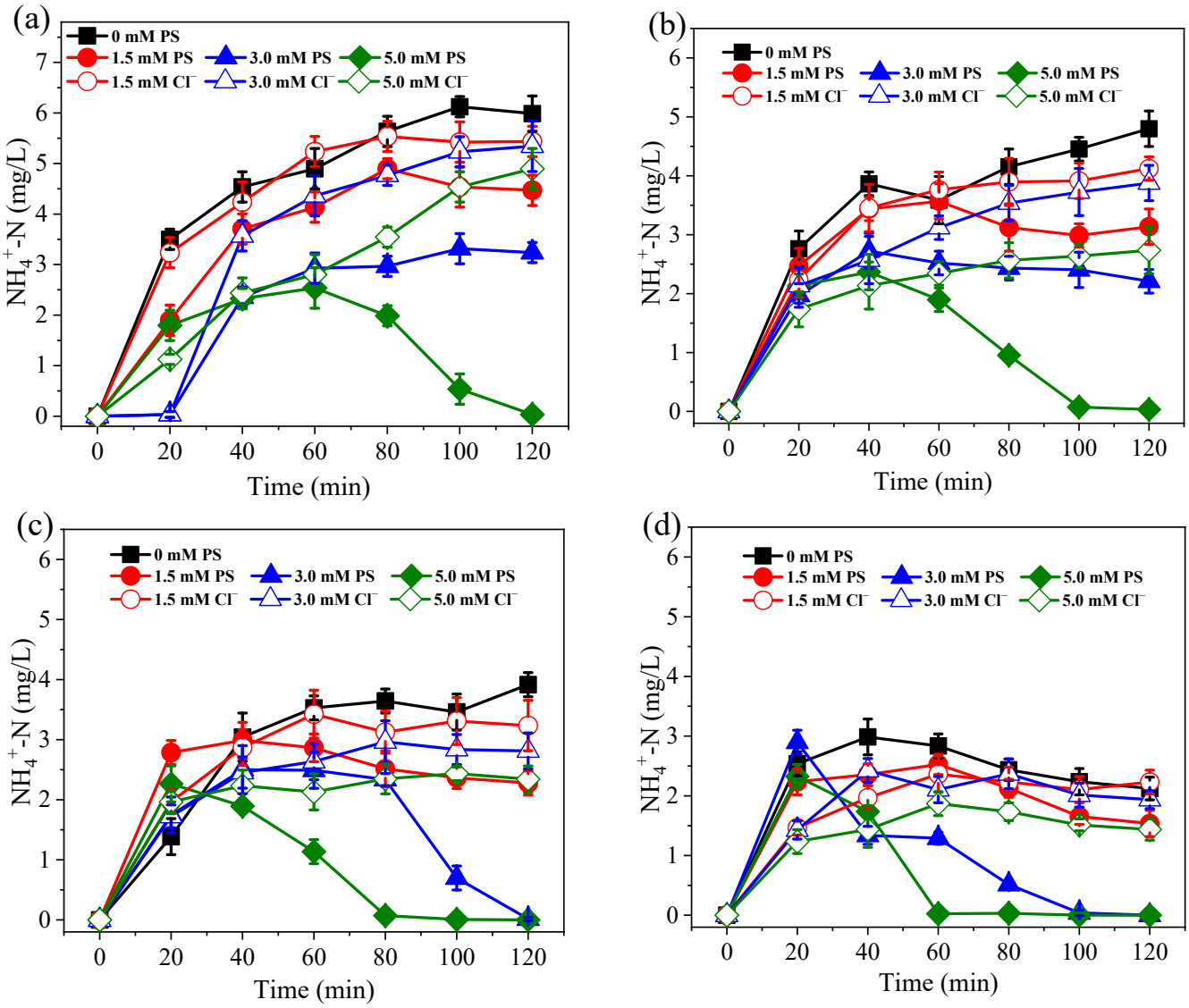

Figure 3. Variation of NH_4^+-N concentration under currents of 0.1 A (**a**), 0.2 A (**b**), 0.3 A (**c**), and 0.4 A (**d**). The dosage of PS and Cl^- were all set at 1.5–5.0 mM. Initial NO_3^--N was 20.0 mg/L. The 10.0 mM Na_2SO_4 was used as electrolyte.

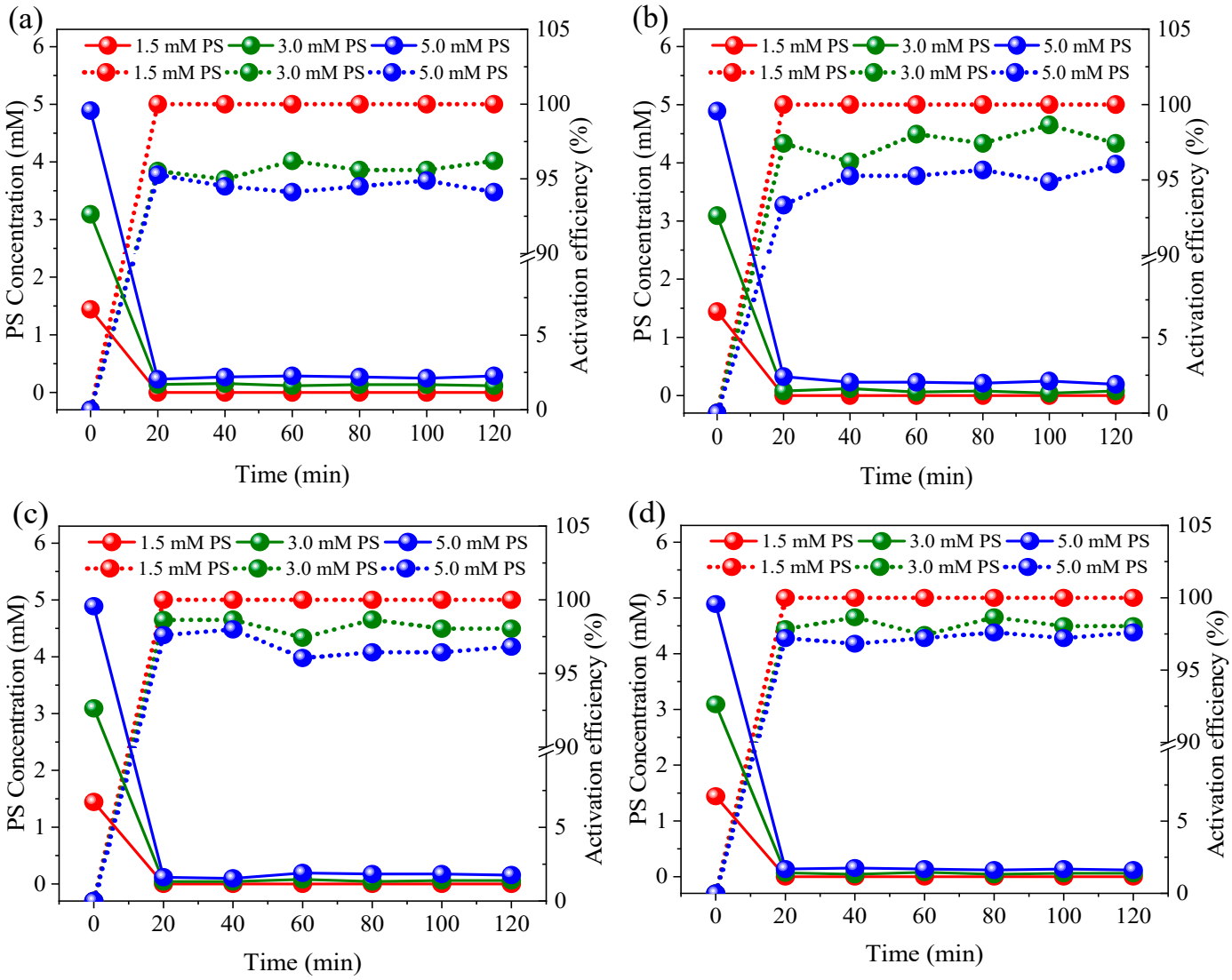

Figure 4. Activation efficiency of PS under currents of 0.1 A (**a**), 0.2 A (**b**), 0.3 A (**c**), and 0.4 A (**d**). Initial PS was 1.5, 3.0 and 5.0 mM. The 10.0 mM Na_2SO_4 was used as electrolyte.

During the treatment processes, all samples dosed with PS achieved lower TN concentrations than the relevant controls (Figure 5). In order to investigate the NH_4^+ oxidation products, samples were prepared by dissolving $(NH_4)_2SO_4$ (6.0 mg/L NH_4^+-N) into 10.0 mM Na_2SO_4, followed by treatment for 120 min at 0.3 A with the addition of 5.0 mM PS. Results showed that only 0.06 mg/L NO_3^--N was generated, while NO_2^--N was undetectable (Figure 6). These results suggest that the oxidation products of NH_4^+ mainly consisted of nitrogenous gases. The release of gaseous substances from aqueous solution resulted in a decrease in TN concentration. When a PS dosage of 5.0 mM was applied, a TN removal efficiency of >99% could be achieved, even at 0.1 and 0.2 A. In contrast, the maximum TN removal efficiency achieved with the addition of 5.0 mM Cl^-, was only 89% at 0.4 A. Therefore, due to the high removal effects achieved under low currents, the oxidation of NH_4^+ by PS not only improves the denitrification efficiency of the system, but also reduces the energy consumption requirements.

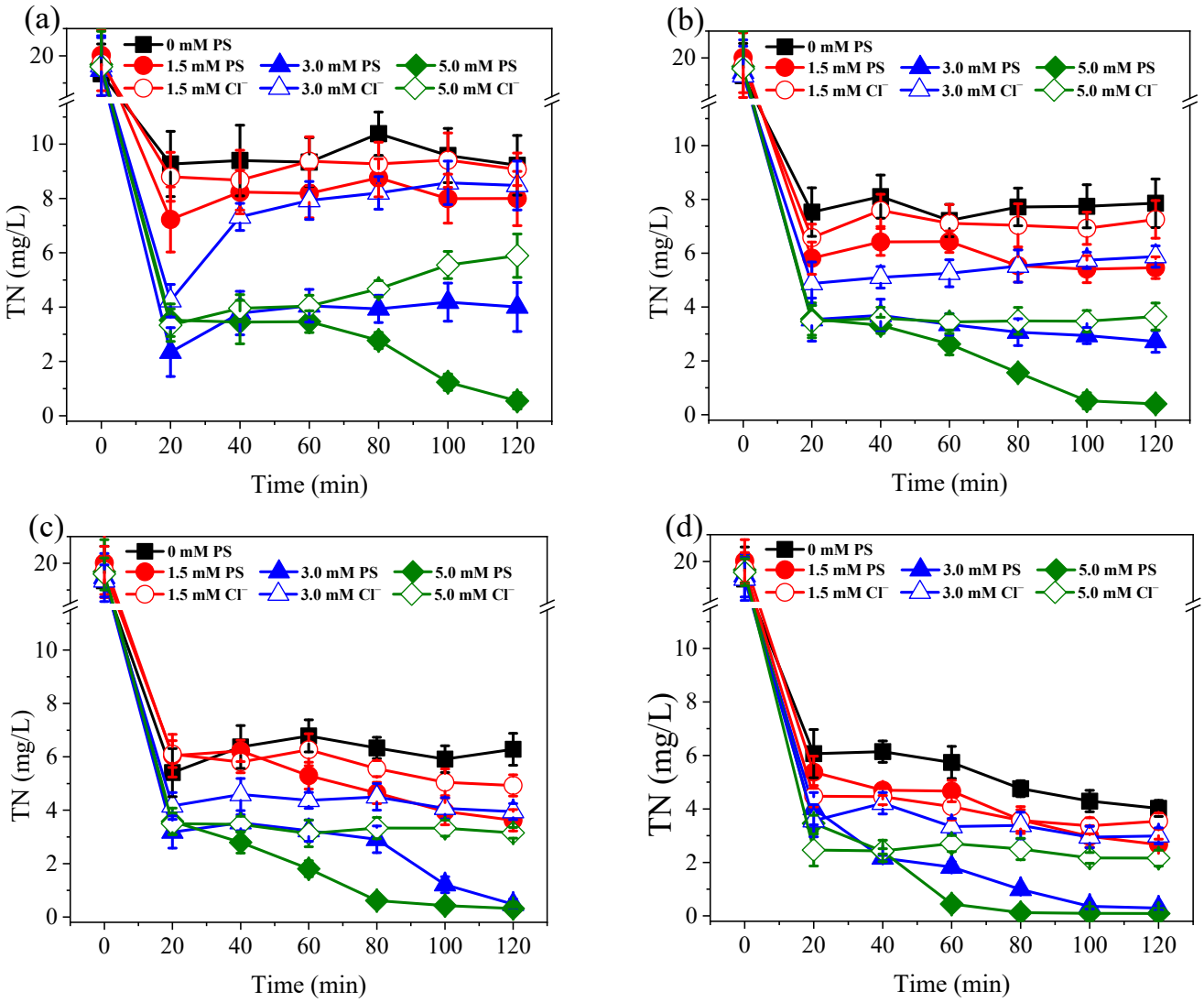

Figure 5. Variation of TN concentration under currents of 0.1 A (**a**), 0.2 A (**b**), 0.3 A (**c**), and 0.4 A (**d**). The dosage of PS and Cl^- were all set at 1.5–5.0 mM. Initial NO_3^--N was 20 mg/L. The 10.0 mM Na_2SO_4 was used as electrolyte.

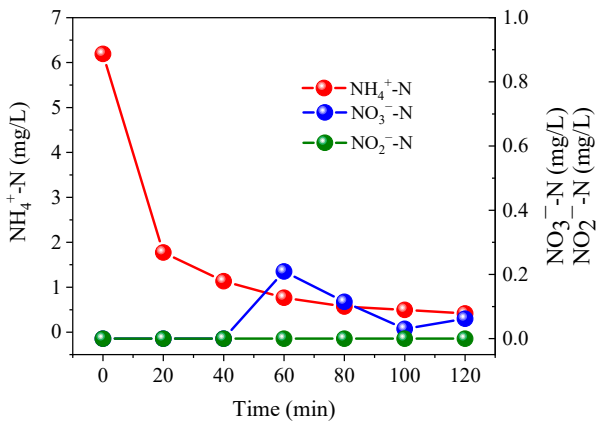

Figure 6. Variation of NO_3^--N, NO_2^--N and NH_4^+-N concentration under 0.3 A with 5.0 mM PS. Initial NH_4^+-N was 6.0 mg/L. The 10.0 mM Na_2SO_4 was used as electrolyte.

3.2. Effects of Coexisting Substances

Various coexisting anions and organic compounds are present in actual municipal sewage. Therefore, the effects of several commonly coexisting species, including PO_4^{3-}, CO_3^{2-} and HA, were investigated. As shown in Figures 7–9, the coexistence of PO_4^{3-}, CO_3^{2-} and HA had a negative impact on the reduction of NO_3^-, especially in terms of the oxidation of NH_4^+. PO_4^{3-} and CO_3^{2-} have been shown to adsorb the surface of electrodes, resulting in competition for active sites and interfering with the adsorption and conversion of NO_3^- [38,39]. HA is an amphoteric substance that can be directly or indirectly reduced on the surface of $Co/AC_{0.9}$-$AB_{0.1}$ particle electrodes, with both systems interfering with the reduction of NO_3^- [22]. During the oxidation of NH_4^+, HPO_4^{2-} (hydrolyzed by PO_4^{3-}) and CO_3^{2-} often act as scavengers of the free radicals $SO_4^{\bullet-}$ and •OH, therefore reacting with $SO_4^{\bullet-}$ and •OH to yield weak oxidants, such as $HPO_4^{\bullet-}$ and $CO_3^{\bullet-}$ (Equations (2)–(5)) [39].

$$SO_4^{\bullet-} + HPO_4^{2-} \rightarrow SO_4^{2-} + HPO_4^{\bullet-} \quad (2)$$

$$\bullet OH + HPO_4^{2-} \rightarrow HPO_4^{\bullet-} + OH^- \quad (3)$$

$$SO_4^{\bullet-} + CO_3^{2-} \rightarrow SO_4^{2-} + CO_3^{\bullet-} \quad (4)$$

$$\bullet OH + CO_3^{2-} \rightarrow OH^- + CO_3^{\bullet-} \quad (5)$$

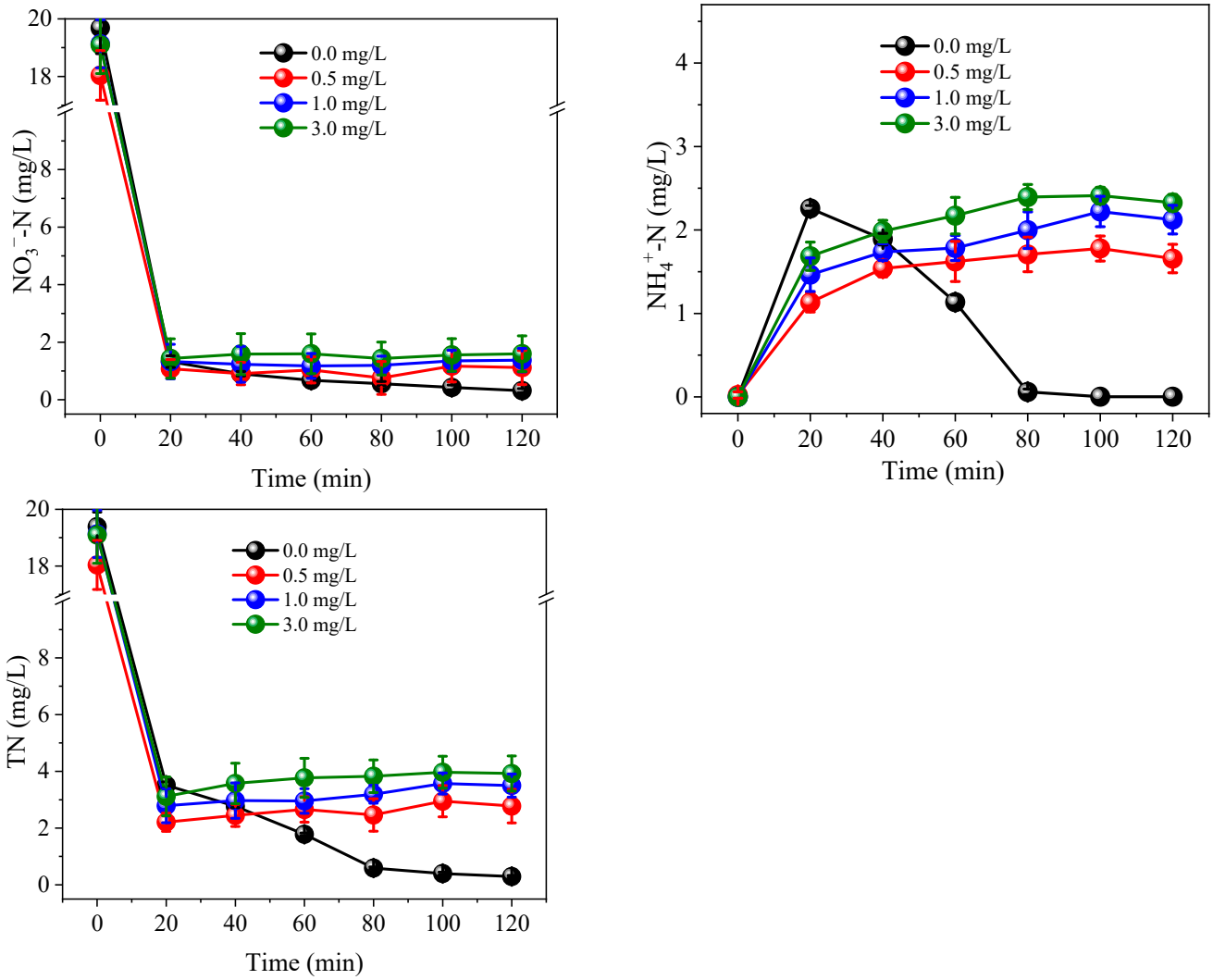

Figure 7. Effects of PO_4^{3-} on the removal of NO_3^--N, NH_4^+-N and TN. Initial NO_3^--N was 20.0 mg/L. Current = 0.3 A. PS = 5.0 mM. The 10.0 mM Na_2SO_4 was used as electrolyte.

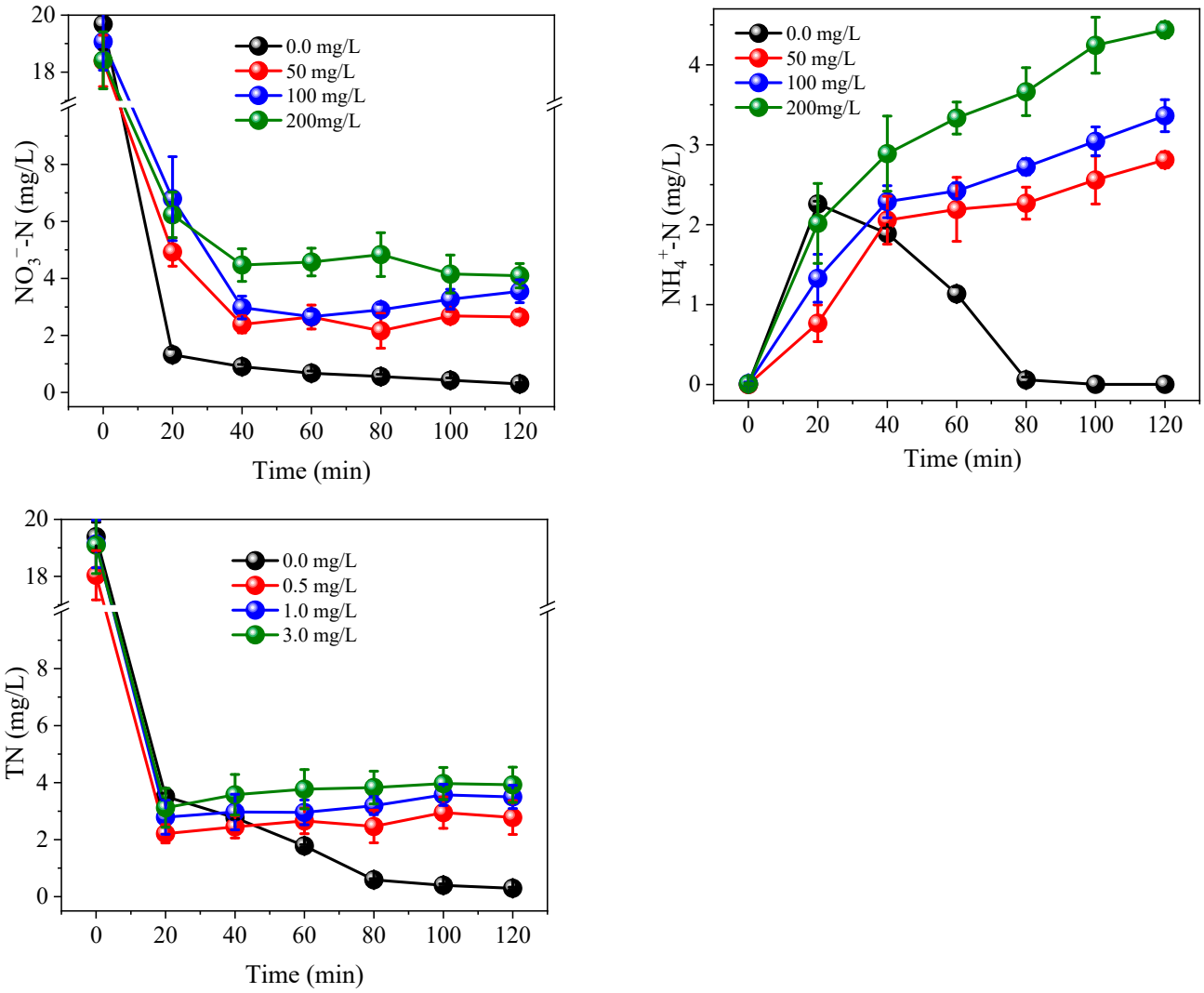

Figure 8. Effects of CO_3^{2-} on the removal of NO_3^--N, NH_4^+-N and TN. Initial NO_3^--N was 20.0 mg/L, current = 0.3 A, PS = 5.0 mM. The 10.0 mM Na_2SO_4 was used as electrolyte.

Similarly, HA can also be oxidized by consuming $SO_4^{\bullet-}$ and •OH [36]. Therefore, the coexistence of these substances reduced the oxidation performance of the radical-based system. The oxidation of NH_4^+ was greatly affected and the efficiency of NO_3^- and NH_4^+ removal was reduced, negatively affecting TN removal. However, after actual sewage treatment, the TP content of the effluent typically ranges from 0.5–1.0 mg/L, while the concentration of HA, expressed as COD, is generally less than 50.0 mg/L [40] and therefore, the concentration of NH_4^+-N would be below 2.0 mg/L under this coexisting substance concentration, which would not adversely affect the water environment. Even if the concentration of CO_3^{2-}-C reached 50.0 mg/L, a concentration of NH_4^+-N in the effluent would measure 2.8 mg/L, which would only have a slight influence on the water environment. However, the negative impact can be mitigated by increasing the PS concentration accordingly.

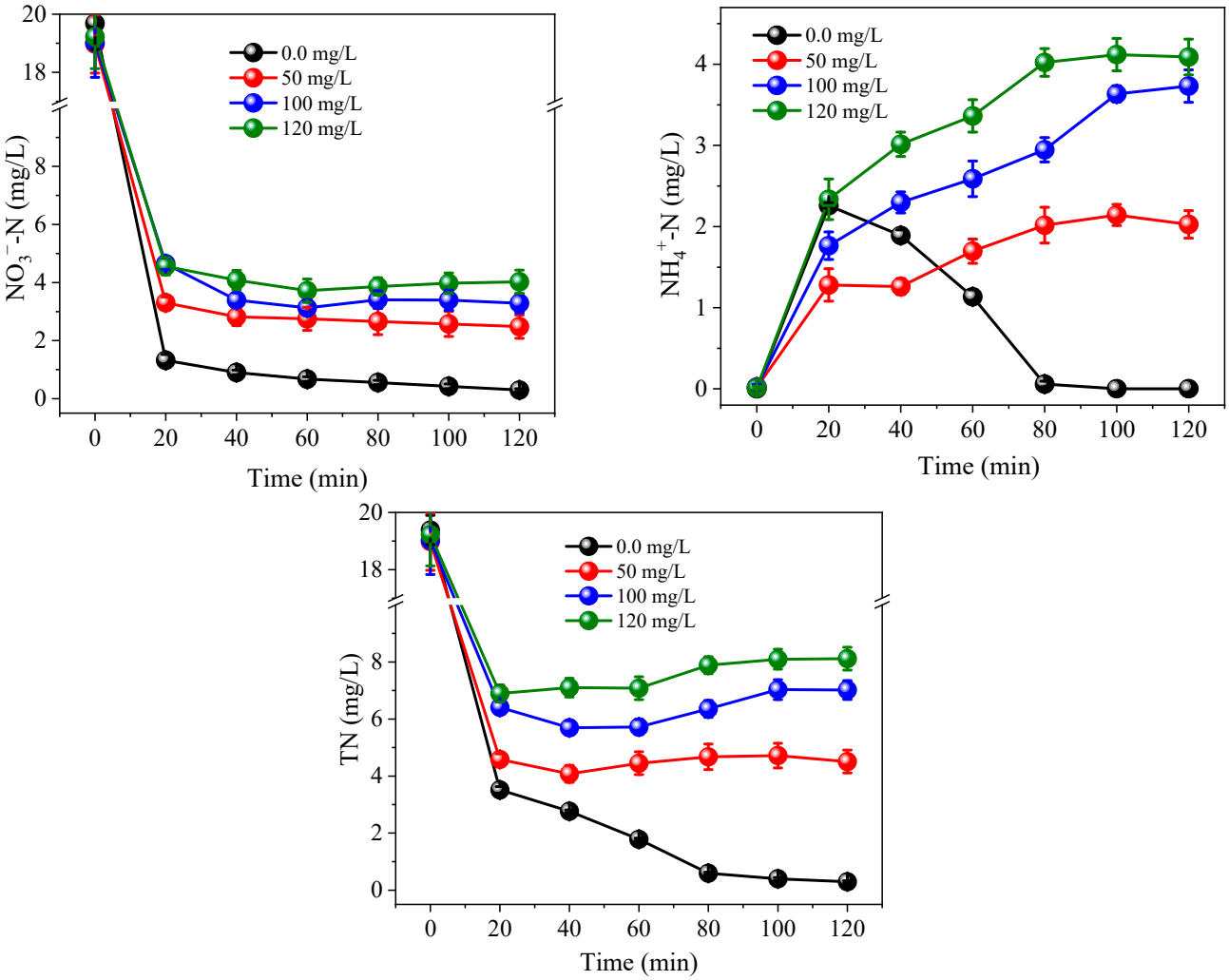

Figure 9. Effects of humic acid on the removal of NO_3^--N, NH_4^+-N and TN. Initial NO_3^--N was 20.0 mg/L, current = 0.3 A, PS = 5.0 mM. The 10.0 mM Na_2SO_4 was used as electrolyte.

3.3. Reactive Species Identification

In order to confirm the active radical species in the PS-Co/$AC_{0.9}$-$AB_{0.1}$ system, ESR experiments were carried out under different conditions. As shown in Figure 10, there were no free radical signals detected in the 2D system. After the addition of PS (2D + PS), a weak signal was observed for the DMPO-SO_4 adduct (1:1:1:1:1:1, a_N = 13.2 G, a_H = 9.5 G, a_N = 1.4 G, a_H = 0.8 G), whereas the DMPO-OH adduct signal (1:2:2:1, a_N = a_H = 14.9 G) was much stronger. This suggests that DMPO-SO_4 and DMPO-OH were both generated from the activation of PS, while the •OH radical was yielded from $SO_4^{\bullet-}$ reacting with H_2O/OH^-, as shown in Equations (6) and (7) [39]:

$$SO_4^{\bullet-} + OH^- \rightarrow \bullet OH + SO_4^{2-} \quad (6)$$

$$SO_4^{\bullet-} + OH^- \rightarrow \bullet OH + SO_4^{2-} \quad (7)$$

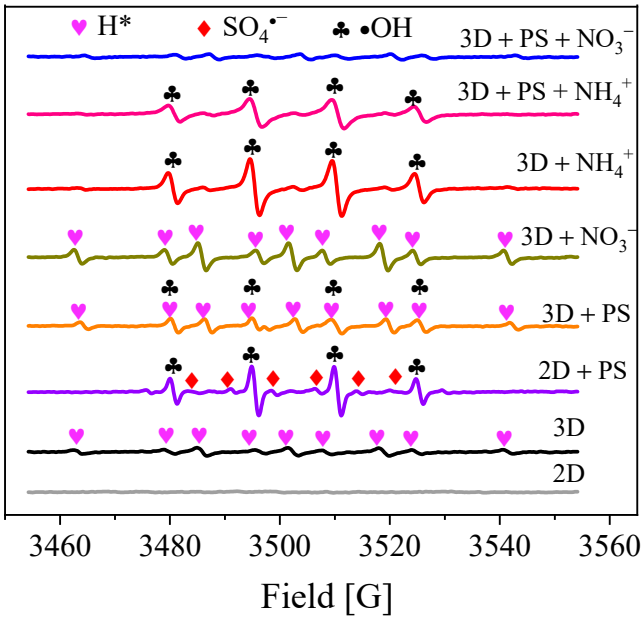

Figure 10. ESR spectra of electrolysis using DMPO spin-trapping under different systems. Current = 0.3 A, PS = 5.0 mM, DMPO = 50.0 mM.

For the 3D system, a weak signal was observed for the DMPO-H adduct (1:1:2:1:2:1:2:1:1), with hyperfine coupling constants of a_N = 15.5 G and a_H = 20.6 G. This indicated that Co/$AC_{0.9}$-$AB_{0.1}$ particle electrodes had performed hydro-reduction of NO_3^-. Atomic H* was generated by the electrolysis of H_2O with catalytically active Co on the particle electrode [22]. After the addition of PS (3D + PS), a new adduct signal (1:2:2:2:2:2:2:2:1) was observed, which was ascribed to the original signal of DMPO-H overlapped with that of DMPO-OH [36]. However, the signal for DMPO-OH was weaker than that of the 2D + PS system, which was due to neutralization of the generated H* and •OH. Moreover, the DMPO-SO_4 signal was too weak to be detected in the 3D + PS system, which can be ascribed to the much higher reaction rate constant between •OH and DMPO compared to between $SO_4^{\bullet-}$ and DMPO [41].

As seen in Figure 10, after NO_3^- was added to the 3D system (3D + NO_3^-), rather than disappearing, the DMPO-H signal was slightly strengthened. This implies that the generation rate and the amount of atomic H* in the 3D system was large enough to reduce NO_3^-. When NH_4^+ was added to the 3D system (3D + NH_4^+), the DMPO-H signal disappeared and a signal for DMPO-OH emerged. As for the 3D + PS + NH_4^+ system, the DMPO-OH signal weakened slightly thereafter, although it remained consistently strong. Although DMPO-OH was generated in both 3D + NH_4^+ and 3D + PS + NH_4^+ systems, the NH_4^+ removal efficiencies of these two systems were apparently different. NH_4^+ could not be effectively oxidized and removed in the 3D system, while in the 3D + PS system NH_4^+ was completely oxidized and removed. Although the DMPO-SO_4 signal was not observed in the 3D + PS system, $SO_4^{\bullet-}$ and •OH can interconvert, with •OH being transferred to $SO_4^{\bullet-}$ via the assistance of SO_4^{2-} and HSO_4^- (Equations (8) and (9)) [31,42]. Furthermore, the slow reaction rate constant for •OH and NH_3/NH_4^+ led to the low level of NH_3/NH_4^+ oxidation by •OH [26,43]. Therefore, it can be inferred that the oxidation of NH_4^+ occurred mainly through its reaction with $SO_4^{\bullet-}$ in the 3D + PS system, resulting in the NH_4^+-N concentration measuring below the detection limit (0.04 mg/L).

$$\bullet OH + SO_4^{2-} \rightarrow SO_4^{\bullet-} + OH^- \quad (8)$$

$$\bullet OH + HSO_4^- \rightarrow SO_4^{\bullet-} + H_2O \quad (9)$$

As shown in Figure 10, nearly no free radical signals could be detected in the 3D + PS + NO_3^- system. The disappearance of the DMPO-H signal indicated hydro-reduction of

NO_3^-, while disappearance of the signals for DMPO-OH and DMPO-SO_4 occurred as a result of consumption of NH_4^+ produced from the electro-reduction of NO_3^-. In addition, due to the reaction of $SO_4^{\bullet-}$ with NH_4^+, more •OH was converted into $SO_4^{\bullet-}$, further weakening the DMPO-OH signal.

3.4. Identification of Dominant Radical

In order to establish the relative contributions from $SO_4^{\bullet-}$ and •OH in the oxidation of NH_4^+, free radical quenching experiments were conducted. TBA is typically used as a scavenger of •OH, as the second reaction rate (k) of $k_{\bullet OH}$ ((3.8–7.6) × 10^8 $M^{-1}s^{-1}$) is about 1000-fold greater than that of $k_{SO_4^{\bullet-}}$ ((4.0–9.4) × 10^5 $M^{-1}s^{-1}$) [44]. EtOH and phenol can both effectively scavenge •OH and $SO_4^{\bullet-}$ with rate constants of $k_{\bullet OH/EtOH}$ = (1.2–2.8) × 10^9 $M^{-1}s^{-1}$, $k_{SO_4^{\bullet-}/EtOH}$ =(1.6–7.7) × 10^7 $M^{-1}s^{-1}$, $k_{\bullet OH/phenol}$ = 6.6 × 10^9 $M^{-1}s^{-1}$ and $k_{SO_4^{\bullet-}/phenol}$ = 8.8 × 10^9 $M^{-1}s^{-1}$ [42,45]. As shown in Figure 11, the NH_4^+ removal efficiency reached 93.3% without the addition of a quenching agent. When the molar ratio of TBA/PS was 1000:1, NH_4^+ removal was inhibited and reduced to 80.7%, indicating •OH had participated in the oxidation of NH_4^+. When the molar ratio of phenol to PS was 200:1, NH_4^+ removal decreased sharply to 45.3%. The number of radicals necessary for TBA to quench oxidation is approximately consistent with phenol [36]. However, the inhibition of NH_4^+ oxidation caused by the addition of a 200:1 molar ratio of phenol was greater than that of 1000:1 molar ratio of TBA, indicating that the contribution of $SO_4^{\bullet-}$ was much greater than that of •OH. Therefore, it can be concluded that $SO_4^{\bullet-}$ played a dominant role in the oxidation of NH_4^+, while the contribution from •OH was less.

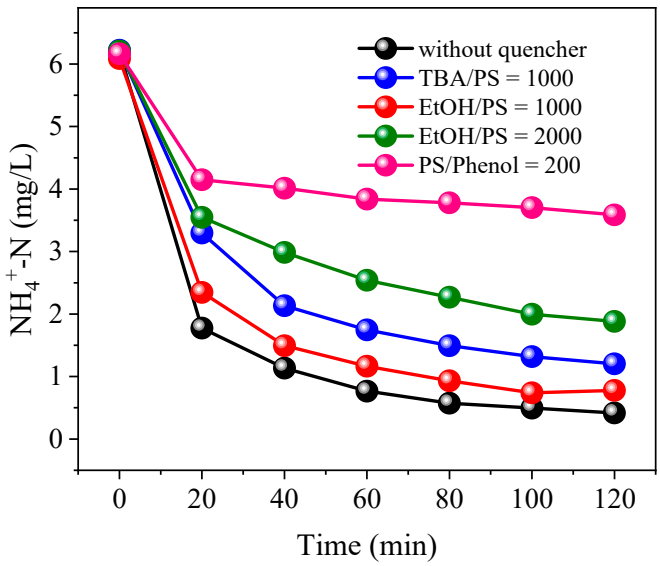

Figure 11. Variation of NH_4^+-N concentrations under PS-Co/$AC_{0.9}$-$AB_{0.1}$ system with different molar ratios of TBA/PS, EtOH/PS and phenol/PS. Current = 0.3 A. PS = 5.0 mM. HRT = 60 min. Initial NH_4^+-N = 6.0 mg/L. The 10.0 mM Na_2SO_4 was used as electrolyte.

Although EtOH can effectively scavenge both $SO_4^{\bullet-}$ and •OH, the addition of EtOH (molar ratio to PS of 1000:1) caused only a 6.0% reduction in NH_4^+ oxidation (Figure 11). Increasing the EtOH/PS molar ratio to 2000:1 increased the suppression of NH_4^+ oxidation to 23.6%. The varied inhibitory effect of the three quenching agents was related to their physicochemical properties and the formation sites of the free radicals [46]. Phenol, TBA and EtOH have varying dielectric constants of 9.78, 12.47 and 28.40, respectively [47]. Dielectric constants reflect the polarity of a substance. Since the polarity of a substance usually reflects its water solubility, the hydrophobic quality of the quenching agents can be ranked in the descending order of phenol > TBA > EtOH. Generally, hydrophobic quenching agents easily react with free radicals present on the surface of catalytic materials.

Powder activated carbon has the property of highly selective adsorption of hydrophobic organic compounds [48]. Therefore, the hydrophobic phenol can more easily approach the particle electrode surface and react with surface-bound free radicals, while hydrophilic TBA and EtOH prefer to compete for •OH and $SO_4^{\bullet-}$ in the liquid phase [47,49]. The greater inhibitory effect of phenol compared to TBA and EtOH, indicates that a majority of •OH and $SO_4^{\bullet-}$ were accumulated on the surface of particle electrodes, with the free radical reaction with NH_4^+ mainly occurring in the boundary layer on the surface of $Co/AB_{0.9}$-$AC_{0.1}$.

3.5. Electrocatalytic Performance of PS-Co/$AC_{0.9}$-$AB_{0.1}$

The PS-$Co/AC_{0.9}$-$AB_{0.1}$ redox process of electrocatalytic denitrification was investigated via CV analysis, with all tests based on the Na_2SO_4 electrolyte. As shown in Figure 12a, only one oxidation peak was observed in the Na_2SO_4 electrolyte at a potential (E_p) of 1.44 V, which was ascribed to the oxidation of Co^0 to Co^{2+}/Co^{3+} [50]. However, no peak was observed for the reduction of Co^{2+}/Co^{3+} to Co^0 during CV cycles, suggesting that Co^{2+}/Co^{3+} might receive electrons transferred from the power source to the cathode surface through a circuit, resulting in conversion of the Co valence state [22,51]. CV curves are often used to reflect heterogeneous charge transfer from an electrode to an electroactive species, although it cannot determine charge transfer and valency changes inside the electrode [9,52]. Therefore, the conversion of Co^{2+}/Co^{3+} to Co^0 mainly serves as an electron shuttle. When NO_3^- was added to the electrolyte solution, no peak of NO_3^- direct reduction appeared (Figure 12b), indicating that the direct electro-reduction of NO_3^- was difficult, with most NO_3^- reduction occurring via a reaction with atomic H* adsorbed on the surface of the $Co/AC_{0.9}$-$AB_{0.1}$ electrode.

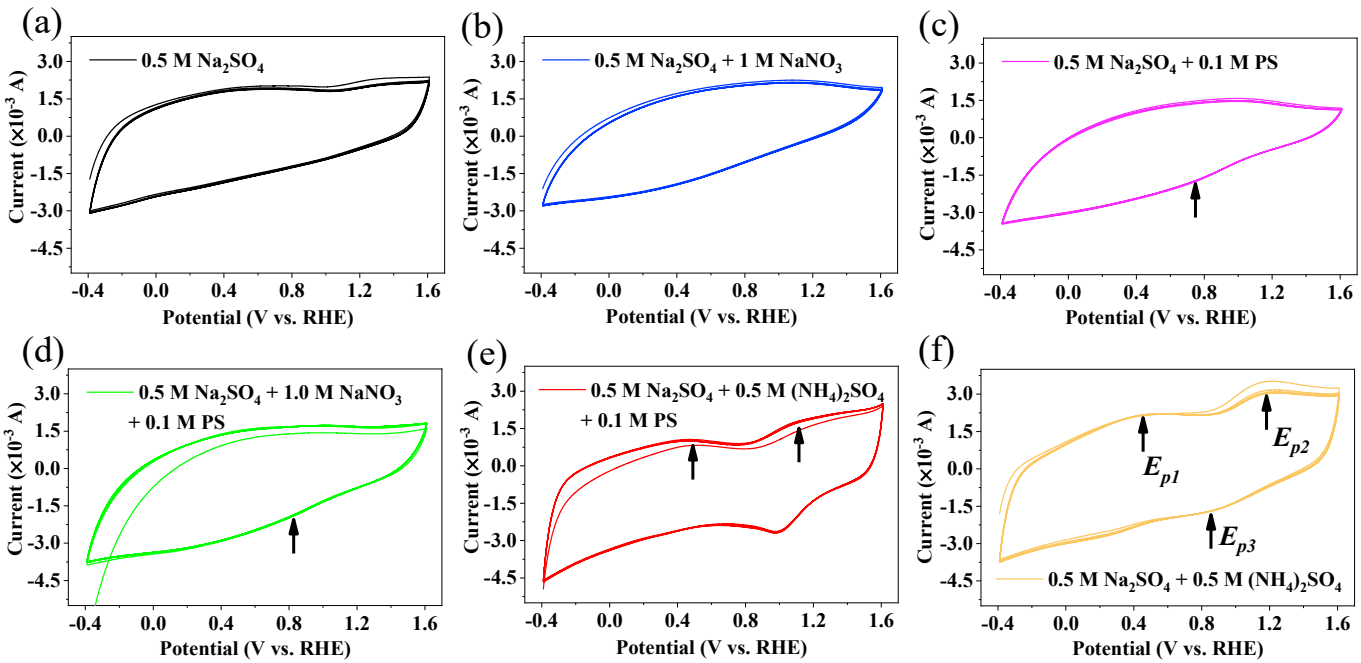

Figure 12. Cyclic voltammetry curves of $Co/AC_{0.9}-AB_{0.1}$ particle electrodes under different electrolyte. 0.5 M Na_2SO_4 (**a**), 0.5M Na_2SO_4 + 1 M $NaNO_3$ (**b**), 0.5 M Na_2SO_4 + 0.1 M PS (**c**), 0.5 M Na_2SO_4 + 1.0 M $NaNO_3$ + 0.1 M PS (**d**), 0.5 MNa_2SO_4 + 0.5 M $(NH_4)_2SO_4$ + 0.1 M PS (**e**) and 0.5 M Na_2SO_4 + 0.5 $(NH_4)_2SO_4$ (**f**). Scan rate = 100 mV/s. Scan for 5 cycles until stable.

When PS was added to the electrolyte solution (Figure 12c), the current response decreased in anodic sweeps. In contrast, the current response increased in cathodic sweeps, indicating the occurrence of strong electron exchange at the electrode, with a weak reduction peak appearing at 0.76 V. Similarly, a reduction peak was observed at 0.83 V in the $NaNO_3$

+ PS system (Figure 12d), with the current also increasing in cathodic sweeps. These peaks were attributed to breakage of the O−O bond of PS [42,53]. The addition of PS promoted the production of atomic H* via the electrolysis of water at the cathode, resulting in an increase in electrode current. In order to establish the PS activation process, CV tests were conducted using different scan rates (v) (Figure 13). As demonstrated in Figure 13a,b, the reduction peak current gradually increased in accordance with the sweep rate, while E_p shifted negatively. E_p was found to be proportional to ln v (R^2 = 0.991), indicating that PS activation was irreversible [54]. The electron transfer number (n) was calculated using the Laviron method (Equation (10)) [55,56]. Based on the CV test results (Figure 13), n value of 1.00 implies that PS activation occurred via a single electron transfer process.

$$E_p = E^o - (RT/\alpha nF)\ln(nF/RTk_s) - (RT/\alpha nF)\ln v \quad (10)$$

where, α represents the electron transfer coefficient; n represents the electron transfer number; k_s is the diffusion coefficient; R is the gas constant (8.315 J/(K·mol); F is the Faraday constant (96,500 C/mol); T is the temperature; and v is the sweep rate.

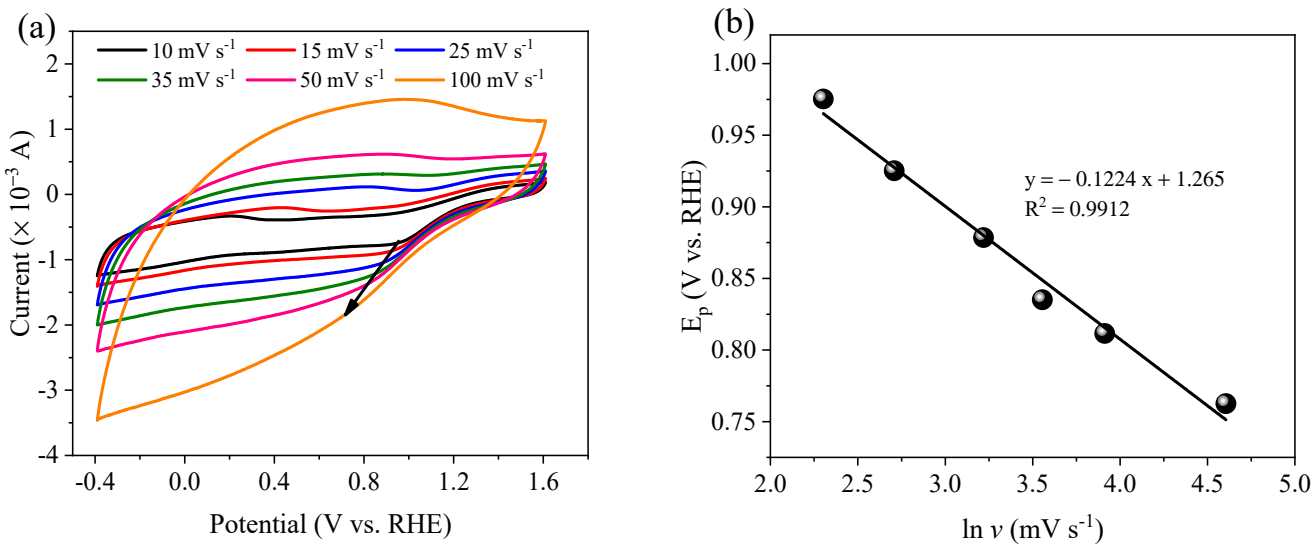

Figure 13. Cyclic voltammetry curves of $Co/AC_{0.9}-AB_{0.1}$ in the 0.1 M Na_2SO_4 + 0.1 M PS at a different scan rate (**a**), and corresponding plot of peak potentials versus the natural logarithm of scan rate in range 10–100 mV s^{-1} (**b**).

As shown in Figure 12f, when $(NH_4)_2SO_4$ was added to the electrolyte solution, two oxidation peaks were observed in the anodic sweeps at 0.42 V (E_{p1}) and 1.18 V (E_{p2}), with electron transfer numbers of 2.86 and 1.00, respectively (Figure 14). As shown in Equations (11)–(13), E_{p1} was considered as the oxidation of NH_3/NH_4^+ to N_2, which involved a three-electron transfer reaction. When N_2 was not rapidly separated from liquid, it was adsorbed by the electrode, causing a single-electron reduction reaction at 0.82 V (E_{p3}) in the cathodic sweep and generating NH_2OH (NH_3OH^+) as an intermediate (Equation (14)) [7]. NH_2OH can also be oxidized into N_2 via single-electron transfer (Equation (15)), resulting in the E_{p2} oxidation peak. When PS was added to the $(NH_4)_2SO_4$ solution (Figure 12e), the peak currents i_{p1} and i_{p2} decreased from 2.18 and 3.09 mA to 1.03 and 1.74 mA, respectively. This occurred due to the generation of $SO_4^{\bullet-}$ and •OH accelerating the NH_4^+ oxidation rate near the electrode surface, resulting in a decrease of NH_4^+-N absorbed on the electrode surface. However, the NH_4^+ in solution could not diffuse to the electrode surface fast enough, weakening the direct oxidation of NH_4^+ and NH_2OH on the electrode and therefore, reducing the current response.

$$NH_3 + H^+ \leftrightarrow NH_4^+ \quad (11)$$

$$NH_3 + 3OH^- - 3e^- \rightarrow 1/2N_2 + 3H_2O \quad (12)$$

$$NH_4^+ - 3e^- \rightarrow 1/2N_2 + 4H^+ \quad (13)$$

$$1/2N_2 + H_2O + 2H^+ + e^- \rightarrow NH_3OH^+ \quad (14)$$

$$NH_2OH + OH^- - e^- \rightarrow 1/2N_2 + 2H_2O \quad (15)$$

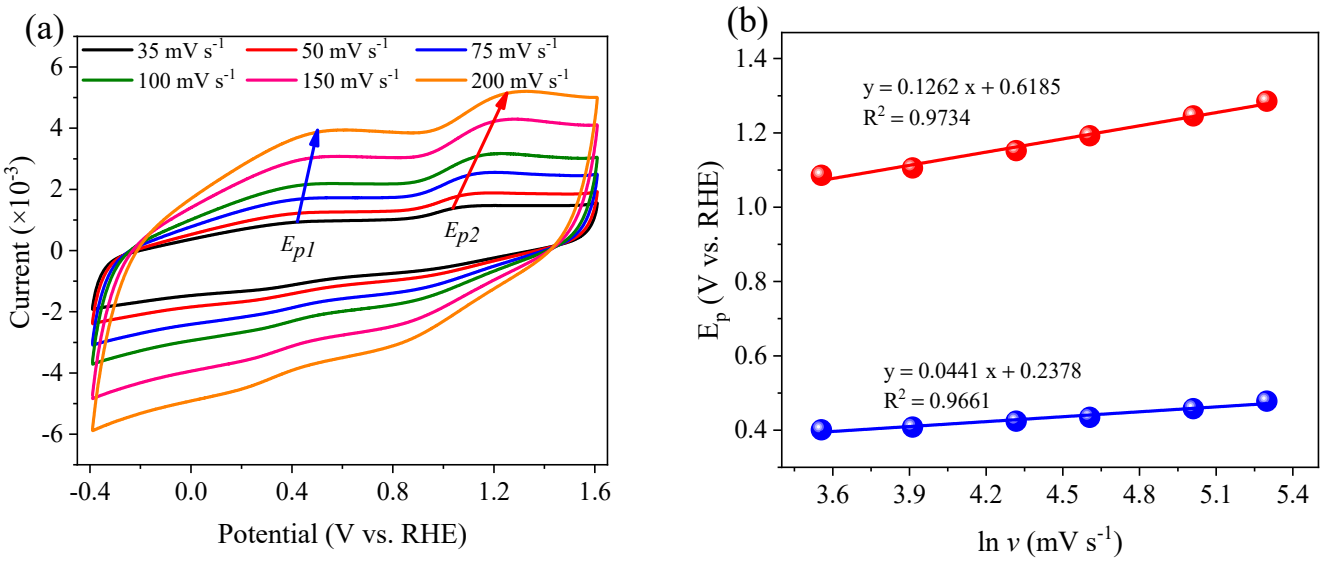

Figure 14. Cyclic voltammetry curves of Co/$AC_{0.9}$-$AB_{0.1}$ in the 0.1 M Na_2SO_4 + 0.5 M $(NH_4)_2SO_4$ at a different scan rate (**a**), and corresponding plot of peak potentials versus the natural logarithm of scan rates in range 35–200 mV s^{-1} (**b**).

3.6. The Mechanism of N Transformation

On the basis of these results, a possible mechanism was proposed for NO_3^- reduction and NH_4^+ oxidation in the PS-Co/$AC_{0.9}$-$AB_{0.1}$ electrocatalytic system (Figure 15). The results of CV test showed that PS activation occurred at the cathode of particle electrodes, generating $SO_4^{\bullet-}$ and subsequently causing •OH to be produced from $SO_4^{\bullet-}$. The process of PS activation occurred via a single electron transfer process, with an activation efficiency of >94.1%. During the electro-reduction process, in our previous study [22], we discovered that when the current was not applied, the nitrate concentration of the effluent was almost unchanged after 60 min of treatment. This implied that the adsorption did not play the main role in the removal of nitrate ions. When the current was applied, NO_3^- was mainly reduced by atomic H*-mediated indirect reduction, with atomic H* produced by electrolysis of H_2O/H^+ via Co catalysis at the particle electrodes. The addition of PS did not interfere with the reduction of NO_3^-, instead promoting the generation of atomic H*, which further promoted the indirect reduction of NO_3^-. The NO_3^- reduction products consisted of nitrogenous gas, NH_4^+ and residual NO_3^-. During the process of electro-oxidation, NH_3/NH_4^+ was directly oxidized via a three-electron reaction at the electrode, generating N_2 as a product. A portion of N_2 was reduced to NH_2OH, which continued to undergo single-electron oxidation. The indirect oxidation of NH_4^+ occurred mainly via $SO_4^{\bullet-}$, while •OH functioned only in assistance. Although the DMPO-OH signal was stronger than that of DMPO-SO_4, the slow reaction rate constant between •OH and NH_4^+ resulted in a poor NH_4^+ removal efficiency. The consumption of $SO_4^{\bullet-}$ could be compensated for by the interconversion between $SO_4^{\bullet-}$ and •OH. The oxidation of NH_4^+ occurred mainly due to radicals accumulated on the surface of particle electrodes, with the products mainly consisting of nitrogenous gas and a small amount of NO_3^-.

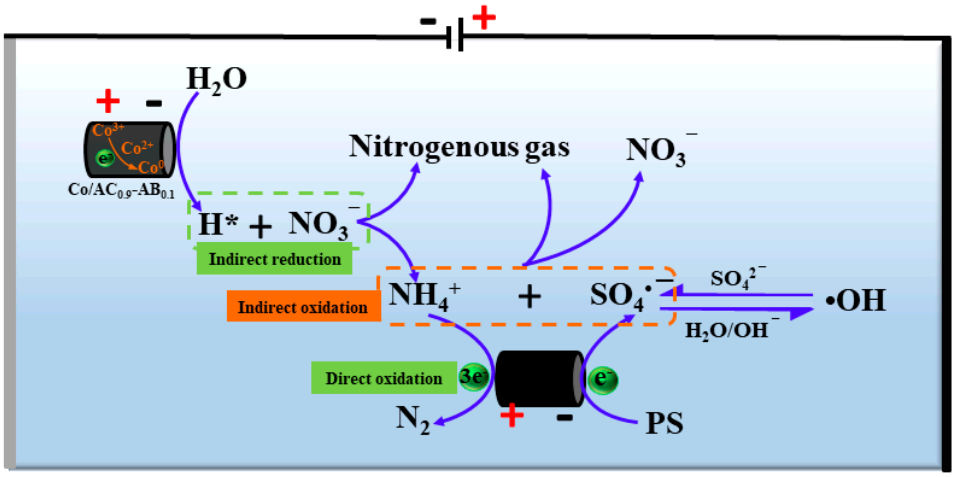

Figure 15. Proposed mechanism of N transformation in PS-Co/$AC_{0.9}$-$AB_{0.1}$ system.

4. Conclusions

Oxidation of the byproduct NH_4^+-N can be achieved using $SO_4^{\bullet-}$-based advanced oxidation under low current conditions, resulting in NH_4^+ being undetectable in the effluent, while also greatly reducing the TN concentration. Compared with active chlorine species, the oxidation of NH_4^+ via $SO_4^{\bullet-}$ species can improve the denitrification efficiency and reduce energy consumption of the treatment system. $SO_4^{\bullet-}$ can be efficiently and easily produced via the single-electron transfer process of PS on the cathodic side of Co/$AC_{0.9}$-$AB_{0.1}$. The PS activation process was found to promote the reduction of NO_3^-, rather than interfere with it. The direct reduction of NO_3^- on the surface of Co/$AC_{0.9}$-$AB_{0.1}$ did not occur easily, with atomic H*-mediated indirect reduction representing the primary pathway of NO_3^- reduction. However, the direct oxidation of NH_4^+ on the Co/$AC_{0.9}$-$AB_{0.1}$ surface can be achieved via a three-electron transfer process, generating N_2 as a product. During the indirect oxidation of NH_4^+, $SO_4^{\bullet-}$ played the dominant role while •OH acted only in assistance. Furthermore, the indirect oxidation of NH_4^+ was primarily accomplished by radicals that had accumulated on the surface of particle electrodes. The NH_4^+ oxidation products mainly consisted of nitrogenous gases, with very small amounts of NO_3^--N and undetectable levels of NO_2^--N present in the effluent. Therefore, the activation of PS using Co/$AC_{0.9}$-$AB_{0.1}$ particle electrodes might be a promising alternative method for oxidizing the byproduct NH_4^+ in the electro-reduction of NO_3^- and reduce TN concentration in advanced sewage treatment.

Author Contributions: Conceptualization, S.Y.; methodology, S.Y. and X.H.; formal analysis, S.Y. and X.H.; investigation, S.Y., W.Z. and Y.L.; resources: S.Y.; data curation, S.Y. and Y.L.; writing—original draft preparation, S.Y.; writing—review and editing, S.Y. and W.L.; visualization, S.Y. and X.Y.; supervision, W.L.; project administration, W.Z. and W.L.; funding acquisition, W.L. All authors have read and agreed to the published version of the manuscript.

Funding: This work was supported by the National Natural Science Foundation of China (Grant No: 51672028), National Water Pollution Control and Management Technology Major Projects of China (Grant No: 2013ZX07209001-003).

Institutional Review Board Statement: Not applicable.

Informed Consent Statement: Not applicable.

Data Availability Statement: Data generated in this study are available upon request.

Acknowledgments: The authors would like to thank the anonymous reviewers and editors for their help in the improvement of this paper.

Conflicts of Interest: The authors declare no conflict of interest.

References

1. Ma, B.; Xu, X.; Ge, S.; Li, B.; Wei, Y.; Zhu, H.; Nan, X.; Peng, Y. Reducing carbon source consumption through a novel denitratation/anammox biofilter to remove nitrate from synthetic secondary effluent. *Bioresour. Technol.* **2020**, *309*, 123377. [CrossRef] [PubMed]
2. Cao, S.; Du, R.; Peng, Y.; Li, B.; Wang, S. Novel two stage partial denitrification (PD)-Anammox process for tertiary nitrogen removal from low carbon/nitrogen (C/N) municipal sewage. *Chem. Eng. J.* **2019**, *362*, 107–115. [CrossRef]
3. Mohajeri, P.; Smith, C.M.S.; Chau, H.W.; Lehto, N. ALLODUST augmented activated sludge single batch anaerobic reactor (AS-SBAnR) for high concentration nitrate removal from agricultural wastewater. *Sci. Total Environ.* **2021**, *752*, 141905. [CrossRef] [PubMed]
4. Su, J.; Kuan, W.-F.; Liu, H.; Huang, C.P. Mode of electrochemical deposition on the structure and morphology of bimetallic electrodes and its effect on nitrate reduction toward nitrogen selectivity. *Appl. Catal. B Environ.* **2019**, *257*, 117909. [CrossRef]
5. Chauhan, R.; Srivastava, V.C. Electrochemical denitrification of highly contaminated actual nitrate wastewater by Ti/RuO_2 anode and iron cathode. *Chem. Eng. J.* **2020**, *386*, 122065. [CrossRef]
6. Liu, Y.; Wang, J. Reduction of nitrate by zero valent iron (ZVI)-based materials: A review. *Sci. Total Environ.* **2019**, *671*, 388–403. [CrossRef]
7. Garcia-Segura, S.; Lanzarini-Lopes, M.; Hristovski, K.; Westerhoff, P. Electrocatalytic reduction of nitrate: Fundamentals to full-scale water treatment applications. *Appl. Catal. B Environ.* **2018**, *236*, 546–568. [CrossRef]
8. Gao, J.; Jiang, B.; Ni, C.; Qi, Y.; Bi, X. Enhanced reduction of nitrate by noble metal-free electrocatalysis on P doped three-dimensional Co_3O_4 cathode: Mechanism exploration from both experimental and DFT studies. *Chem. Eng. J.* **2020**, *382*, 123034. [CrossRef]
9. Gao, J.; Jiang, B.; Ni, C.; Yuanfeng, Q.; Zhang, Y.; Oturan, N.; Oturan, M. Non-precious Co_3O_4-TiO_2/Ti cathode based electrocatalytic nitrate reduction: Preparation, performance and mechanism. *Appl. Catal. B Environ.* **2019**, *254*, 391–402. [CrossRef]
10. Jin, J.; Wang, Y.; Wu, Z.; Hergazy, A.; Lan, J.; Zhao, L.; Liu, X.; Chen, N.; Lin, L. Transcriptomic analysis of liver from grass carp (*Ctenopharyngodon idellus*) exposed to high environmental ammonia reveals the activation of antioxidant and apoptosis pathways. *Fish Shellfish Immunol.* **2017**, *63*, 444–451. [CrossRef]
11. Martínez, J.; Ortiz, A.; Ortiz, I. State-of-the-art and perspectives of the catalytic and electrocatalytic reduction of aqueous nitrates. *Appl. Catal. B Environ.* **2017**, *207*. [CrossRef]
12. Dima, G.E.; de Vooys, A.C.A.; Koper, M.T.M. Electrocatalytic reduction of nitrate at low concentration on coinage and transition-metal electrodes in acid solutions. *J. Electroanal. Chem.* **2003**, *554–555*, 15–23. [CrossRef]
13. Dash, B.P.; Chaudhari, S. Electrochemical denitrificaton of simulated ground water. *Water Res.* **2005**, *39*, 4065–4072. [CrossRef]
14. Reyter, D.; Belanger, D.; Roue, L. Nitrate removal by a paired electrolysis on copper and Ti/IrO_2 coupled electrodes—Influence of the anode/cathode surface area ratio. *Water Res.* **2010**, *44*, 1918–1926. [CrossRef]
15. Mácová, Z.; Bouzek, K.; Šerák, J. Electrocatalytic activity of copper alloys for NO_3^- reduction in a weakly alkaline solution. *J. Appl. Electrochem.* **2007**, *37*, 557–566. [CrossRef]
16. Reyter, D.; Bélanger, D.; Roué, L. Elaboration of Cu–Pd Films by Coelectrodeposition: Application to Nitrate Electroreduction. *J. Phys. Chem. C* **2008**, *113*, 290–297. [CrossRef]
17. Birdja, Y.Y.; Yang, J.; Koper, M.T.M. Electrocatalytic Reduction of Nitrate on Tin-modified Palladium Electrodes. *Electrochim. Acta* **2014**, *140*, 518–524. [CrossRef]
18. Comisso, N.; Cattarin, S.; Guerriero, P.; Mattarozzi, L.; Musiani, M.; Vázquez-Gómez, L.; Verlato, E. Study of Cu, Cu-Ni and Rh-modified Cu porous layers as electrode materials for the electroanalysis of nitrate and nitrite ions. *J. Solid State Electrochem.* **2015**, *20*, 1139–1148. [CrossRef]
19. Lan, H.; Liu, X.; Liu, H.; Liu, R.; Hu, C.; Qu, J. Efficient Nitrate Reduction in a Fluidized Electrochemical Reactor Promoted by Pd–Sn/AC Particles. *Catal. Lett.* **2015**, *146*, 91–99. [CrossRef]
20. Fan, J.; Xu, H.; Lv, M.; Wang, J.; Teng, W.; Ran, X.; Gou, X.; Wang, X.; Sun, Y.; Yang, J. Mesoporous carbon confined palladium–copper alloy composites for high performance nitrogen selective nitrate reduction electrocatalysis. *New J. Chem.* **2017**, *41*, 2349–2357. [CrossRef]
21. Wang, Q.; Huang, H.; Wang, L.; Chen, Y. Electrochemical removal of nitrate by Cu/Ti electrode coupled with copper-modified activated carbon particles at a low current density. *Environ. Sci. Pollut. Res. Int.* **2019**, *26*, 17567–17576. [CrossRef]
22. Ye, W.; Zhang, W.; Hu, X.; Yang, S.; Liang, W. Efficient electrochemical-catalytic reduction of nitrate using Co/$AC_{0.9}$-$AB_{0.1}$ particle electrode. *Sci. Total Environ.* **2020**, *732*, 139245. [CrossRef]
23. Sun, W.; Sun, Y.; Shah, K.J.; Chiang, P.C.; Zheng, H. Electrocatalytic oxidation of tetracycline by Bi-Sn-Sb_γ-Al_2O_3 three-dimensional particle electrode. *J. Hazard. Mater.* **2019**, *370*, 24–32. [CrossRef]
24. Mandal, P.; Yadav, M.K.; Gupta, A.K.; Dubey, B.K. Chlorine mediated indirect electro-oxidation of ammonia using non-active PbO_2 anode: Influencing parameters and mechanism identification. *Sep. Purif. Technol.* **2020**, *247*, 116910. [CrossRef]
25. Devi, P.; Dalai, A.K. Implications of breakpoint chlorination on chloramines decay and disinfection by-products formation in brine solution. *Desalination* **2021**, *504*, 114961. [CrossRef]
26. Huang, L.; Li, L.; Dong, W.; Liu, Y.; Hou, H. Removal of Ammonia by OH Radical in Aqueous Phase. *Environ. Sci.Technol.* **2008**, *42*, 8070–8075. [CrossRef]

27. Wacławek, S.; Lutze, H.V.; Grübel, K.; Padil, V.V.T.; Černík, M.; Dionysiou, D.D. Chemistry of persulfates in water and wastewater treatment: A review. *Chem. Eng. J.* **2017**, *330*, 44–62. [CrossRef]
28. Van Berkel, K.Y.; Russell, G.T.; Gilbert, R.G. The dissociation rate coefficient of persulfate in emulsion polymerization systems. *Polymer* **2006**, *47*, 4667–4675. [CrossRef]
29. Du, X.; Zhou, M. Strategies to enhance catalytic performance of metal-organic frameworks in sulfate radical-based advanced oxidation processes for organic pollutants removal. *Chem. Eng. J.* **2021**, *403*, 126346. [CrossRef]
30. Huang, J.; Zhang, H. Mn-based catalysts for sulfate radical-based advanced oxidation processes: A review. *Environ. Int.* **2019**, *133*, 105141. [CrossRef]
31. Giannakis, S.; Lin, K.-Y.A.; Ghanbari, F. A review of the recent advances on the treatment of industrial wastewaters by Sulfate Radical-based Advanced Oxidation Processes (SR-AOPs). *Chem. Eng. J.* **2021**, *406*, 127083. [CrossRef]
32. Chen, C.; Feng, H.; Deng, Y. Re-evaluation of sulfate radical based-advanced oxidation processes (SR-AOPs) for treatment of raw municipal landfill leachate. *Water Res.* **2019**, *153*, 100–107. [CrossRef] [PubMed]
33. Zhang, F.; Sun, Z.; Cui, J. Research on the mechanism and reaction conditions of electrochemical preparation of persulfate in a split-cell reactor using BDD anode. *RSC Adv.* **2020**, *10*, 33928–33936. [CrossRef]
34. Qing, G.; Ghazfar, R.; Jackowski, S.T.; Habibzadeh, F.; Ashtiani, M.M.; Chen, C.P.; Smith, M.R., 3rd; Hamann, T.W. Recent Advances and Challenges of Electrocatalytic N_2 Reduction to Ammonia. *Chem. Rev.* **2020**, *120*, 5437–5516. [CrossRef]
35. Liang, C.; Huang, C.-F.; Mohanty, N.; Kurakalva, R.M. A rapid spectrophotometric determination of persulfate anion in ISCO. *Chemosphere* **2008**, *73*, 1540–1543. [CrossRef]
36. Zhang, W.; He, Y.; Li, C.; Hu, X.; Yang, S.; You, X.; Liang, W. Persulfate activation using Co/AC particle electrodes and synergistic effects on humic acid degradation. *Appl. Catal. B Environ.* **2021**, *285*, 119848. [CrossRef]
37. Yan, Z.; Zheng, X.; Fan, J.; Zhang, Y.; Wang, S.; Zhang, T.; Sun, Q.; Huang, Y. China national water quality criteria for the protection of freshwater life: Ammonia. *Chemosphere* **2020**, *251*, 126379. [CrossRef]
38. Liu, J.; Jiang, S.; Chen, D.; Dai, G.; Wei, D.; Shu, Y. Activation of persulfate with biochar for degradation of bisphenol A in soil. *Chem. Eng. J.* **2020**, *381*, 122637. [CrossRef]
39. Huang, W.; Xiao, S.; Zhong, H.; Yan, M.; Yang, X. Activation of persulfates by carbonaceous materials: A review. *Chem. Eng. J.* **2021**, *418*, 129297. [CrossRef]
40. Wang, X.-H.; Wang, X.; Huppes, G.; Heijungs, R.; Ren, N.-Q. Environmental implications of increasingly stringent sewage discharge standards in municipal wastewater treatment plants: Case study of a cool area of China. *J. Clean. Prod.* **2015**, *94*, 278–283. [CrossRef]
41. Chen, L.; Hu, X.; Cai, T.; Yang, Y.; Zhao, R.; Liu, C.; Li, A.; Jiang, C. Degradation of Triclosan in soils by thermally activated persulfate under conditions representative of in situ chemical oxidation (ISCO). *Chem. Eng. J.* **2019**, *369*, 344–352. [CrossRef]
42. Qi, F.; Zeng, Z.; Wen, Q.; Huang, Z. Enhanced organics degradation by three-dimensional (3D) electrochemical activation of persulfate using sulfur-doped carbon particle electrode: The role of thiophene sulfur functional group and specific capacitance. *J. Hazard. Mater.* **2021**, *416*, 125810. [CrossRef]
43. Zhu, X.; Nanny, M.; Butler, E. Effects of pH and Catalyst Concentration on Photocatalytic Oxidation of Aqueous Ammonia and Nitrite in Titanium Dioxide Suspensions. *Environ.Sci.Technol.* **2005**, *39*, 3784–3791. [CrossRef]
44. Gong, C.; Chen, F.; Yang, Q.; Luo, K.; Yao, F.; Wang, S.; Wang, X.; Wu, J.; Li, X.; Wang, D.; et al. Heterogeneous activation of peroxymonosulfate by Fe-Co layered doubled hydroxide for efficient catalytic degradation of Rhoadmine B. *Chem. Eng. J.* **2017**, *321*, 222–232. [CrossRef]
45. Yang, S.; Yang, X.; Shao, X.; Niu, R.; Wang, L. Activated carbon catalyzed persulfate oxidation of Azo dye acid orange 7 at ambient temperature. *J. Hazard. Mater.* **2011**, *186*, 659–666. [CrossRef]
46. Xu, Y.; Lin, H.; Li, Y.; Zhang, H. The mechanism and efficiency of MnO_2 activated persulfate process coupled with electrolysis. *Sci. Total Environ.* **2017**, *609*, 644–654. [CrossRef]
47. Yan, S.; Xiong, W.; Xing, S.; Shao, Y.; Guo, R.; Zhang, H. Oxidation of organic contaminant in a self-driven electro/natural maghemite/peroxydisulfate system: Efficiency and mechanism. *Sci. Total Environ.* **2017**, *599–600*, 1181–1190. [CrossRef]
48. Oh, H.K.; Takizawa, S.; Ohgaki, S.; Katayama, H.; Oguma, K.; Yu, M.J. Removal of organics and viruses using hybrid ceramic MF system without draining PAC. *Desalination* **2007**, *202*, 191–198. [CrossRef]
49. Liu, Y.; Chen, X.; Yang, Y.; Feng, Y.; Wu, D.; Mao, S. Activation of persulfate with metal–organic framework-derived nitrogen-doped porous Co@C nanoboxes for highly efficient p-Chloroaniline removal. *Chem. Eng. J.* **2019**, *358*, 408–418. [CrossRef]
50. Qian, L.; Gu, L.; Yuan, H.; Xiao, D. Direct growth of $NiCo_2O_4$ nanostructures on conductive substrates with enhanced electrocatalytic activity and stability for methanol oxidation. *Nanoscale* **2013**, *5*, 7388–7396. [CrossRef]
51. Wang, H.; Qing, C.; Guo, J.; Aref, A.A.; Sun, D.; Wang, B.; Tang, Y. Highly conductive carbon–CoO hybrid nanostructure arrays with enhanced electrochemical performance for asymmetric supercapacitors. *J. Mater. Chem. A* **2014**, *2*, 11776–11783. [CrossRef]
52. Li, A.; Zhao, X.; Hou, Y.; Liu, H.; Wu, L.; Qu, J. The electrocatalytic dechlorination of chloroacetic acids at electrodeposited Pd/Fe-modified carbon paper electrode. *Appl. Catal. B Environ.* **2012**, *111–112*, 628–635. [CrossRef]
53. Duan, X.; Su, C.; Zhou, L.; Sun, H.; Suvorova, A.; Odedairo, T.; Zhu, Z.; Shao, Z.; Wang, S. Surface controlled generation of reactive radicals from persulfate by carbocatalysis on nanodiamonds. *Appl. Catal. B Environ.* **2016**, *194*, 7–15. [CrossRef]
54. Hu, X.; Yang, S.; You, X.; Zhang, W.; Liu, Y.; Liang, W. Electrocatalytic Decomplexation of Cu-EDTA and Simultaneous Recovery of Cu with Ni/GO-PAC Particle Electrode. *Chem. Eng. J.* **2021**, *428*, 131468. [CrossRef]

55. Laviron, E. General expression of the linear potential sweep voltammogram in the case of diffusionless electrochemical systems. *J. Electroanal. Chem.* **1979**, *101*, 19–28. [CrossRef]
56. Luong, J.H.T.; Glennon, J.D.; Gedanken, A.; Vashist, S.K. Achievement and assessment of direct electron transfer of glucose oxidase in electrochemical biosensing using carbon nanotubes, graphene, and their nanocomposites. *Microchim. Acta* **2016**, *184*, 369–388. [CrossRef]